www.czasopisma.pan.pl PAN www.journals.pan.pl
Chemical and Process Engineering 2018, 39 (3), 335–345
DOI: 10.24425/122954

INFLUENCE OF LIQUID FLOWRATE ON SIZE OF NANOBUBBLES GENERATED BY POROUS-MEMBRANE MODULES

Karol Ulatowski*, Paweł Sobieszuk

Warsaw University of Technology, Faculty of Chemical and Process Engineering,
Waryńskiego 1, 00-645 Warsaw, Poland

The aim of this work was to investigate the influence of distilled water flowrate in two different porous-membrane modules on the size of generated nitrogen nanobubbles. Modules had different diameter and number of membrane tubes inside the module. As bubbles are cut off from the membrane surface by a shear stress induced by the liquid flow, the change in the linear liquid velocity should result in a change of the generated bubble diameter. For both modules, higher flowrate of liquid induced generation of smaller bubbles, which was consistent with our expectations. This effect can help us in generation of bubbles of desired size.

Keywords: nanobubbles, porous membranes, size distribution

1. INTRODUCTION

Nanotechnology began to be of interest when scientists found means to measure objects in nanoscale. That is when the extraordinary properties of such objects started to be discovered and described. When we begin to decrease the size of an object, starting from macroscale, initially most of its physicochemical properties remain constant. However, when the size approaches nanoscale, the properties start to change linearly or even nonlinearly (Cademartiri et al., 2009). This change is linked to an increasing fraction of atoms located on the surface of the object.

1.1. Nanobubble characteristics

For most of the time, nanotechnological studies were focused on investigation of solid nanoparticles. However, this focus begins to shift in favour of nanoobjects which involve liquids (nanodroplets, nanoemulsions) or gas nanobubbles, which are described further in this paper. Nanobubbles can further be bisected on bulk nanobubbles (which are not adhered to any solid surface and are homogenously dispersed in the liquid) and surface nanobubbles (adhered to the solid surface). In this work, under the term 'nanobubbles', we assume bulk nanobubbles. In case of nanobubbles, the nanoscale starts just under the size of 1 μm, as this is the approximate boundary of rapid change in physicochemical properties of gas bubbles (Tsuge, 2015). Nanobubbles possess extraordinary characteristics which distinguish them from their macroscale counterparts. First of all, nanobubbles have nearly non-existent rising velocity (Li et al., 2014; Tsuge,

* Corresponding author, e-mail: Karol.Ulatowski.dokt@pw.edu.pl
Reprinted with permission in an extended form from the EYEC Monograph accompanying 7th European Young Engineers Conference.

2015) and their paths in liquid can be described by the Brownian motion (Takahashi, 2009; Tsuge, 2015). Such small value of a rising velocity is caused by a very high density of gas within the bubble. High density is caused by a significant pressure difference between inside and outside of a bubble (Li et al., 2014; Tsuge, 2015). This difference is produced by surface tension and can be described by the Young-Laplace equation even for such small bubbles (Matsumoto and Tanaka, 2008):

$$\Delta P = \frac{4\sigma}{d} \tag{1}$$

Such a high pressure difference, if we apply equations relevant to bubbles in macroscale, should result in an almost instantaneous dissolution of bubbles in liquid (Zhang et al., 2008). Surprisingly, nanobubbles are extremely stable and can last unchanged in liquid for days or even months (Takahashi, 2009). Most scientists agree that the main reason for such stability is the presence of electrical charge accumulated on the surface of object (Bunkin et al., 1996). In case of nanobubbles, the mentioned charge results from hydroxyl anions adhesion on the bubble surface. They form a firm layer which impedes the mass transfer and coalescence with surrounding bubbles (Ghosh, 2009; Srinivas and Ghosh, 2012). To overcome this charge external energy must be delivered (Ghosh, 2009) and an amount of the energy can be approximated by zeta potential measurements. The higher the absolute value of zeta potential, the more energy is needed to perform coalescence or mass transfer. The value of absolute zeta potential can be lowered by addition of alcohol or salts (Srinivas and Ghosh, 2012). However, there are numerical simulations which show that the addition of surfactants, which are known to lower the surface tension between gas and liquid, to liquid phase in contact with surface nanobubbles can destabilize bubbles and result in their dissolution (Xiao et al., 2017). That means that both the surface tension and high value of zeta potential are needed to ensure the stability of bubbles.

1.2. Nanobubble applications

Nanobubbles display unexpected usability in various branches of science and industry. For instance, they are commonly used in wastewater treatment, both in biochemical and in mechanical parts of wastewater treatment plants. As for chemical treatment, oxygen bubbles, starting from microscale, have the ability to mass produce hydroxyl radicals. High oxidation potential of radicals is the reason of destruction of various chemical pollutants (Sreekanth et al., 2013; Sunil Paul et al., 2013). When ozone micro- and nanobubbles are generated, even more hydroxyl radicals are produced (Von Gunten, 2003). Bubbles of both oxygen and ozone have the ability to reduce COD of wastewater by even 90% (Kutty et al., 2010). Because of this fact, nanobubbles of these gases were used to reduce the concentration of pesticides in both water and ground originating from heavy polluted fields (Ikeura et al., 2011), as well as to decolorize wastewater by decomposing dyes from textile industry (Chu et al., 2007). In both cases the efficiency of processes under consideration was vastly increased.

In the case of mechanical treatment of wastewater, micro- and nanobubbles are applied in flotation of solid particles and oils. Because of their extremely low rising velocity, bubbles of this scales are able to disperse in the entire volume of the flotation tank and reach zones which cannot be penetrated by bubbles of bigger size (Kutty et al., 2010). The usefulness of bubbles in flotation increases with decreasing bubble diameter. Smaller bubbles can adhere to smaller oil droplets or solid particles. Also, in case of larger droplets and particles, the smaller the bubble diameter, the higher the number of bubbles which can adhere to single droplet or particle. It is important, as the combined drag force of numerous bubbles is able to lift the contaminants to the surface with higher rising velocity than with macrobubbles (Etchepare et al., 2017). When we also consider the fact that freely dispersed nanobubbles have nearly non-existent rising velocity and fill the whole volume of flotation tank, it becomes evident that dispersed bubbles can react immediately to the presence of contaminants (Etchepare et al., 2017).

Micro- and nanobubbles are also used in disinfection by inactivation of bacteria, viruses or yeast cells (Khadre et al., 2001), even when treatment with atmosphere of the same gas proves to be inefficient (Kobayashi et al., 2011). Also, bubbles of these scales can promote growth of plants, fish and animals (Ebina et al., 2013; Park and Kurata, 2009) In every case, treatment with bubble saturated water resulted in higher food intake and bigger size (higher body mass, longer leaves, etc.) (Ebina et al., 2013; Park and Kurata, 2009).

1.3. Nanobubble generation

There are methods used for generation of bulk micro- and nanobubbles, but they are not studied as thoroughly as their applications. In general, generation methods can be divided into three groups, based on main phenomenon that leads to generation: electrolysis of salts (Kikuchi et al., 2006), gas-liquid circulation and compression-decompression methods (Terasaka et al., 2011). During electrolysis of salts gas products are released on the electrodes in form of bubbles in solution. This method leads to producing multimodal distribution of bubble sizes ranging from nanometers to millimeters (Kikuchi et al., 2006). Compression-decompression methods are based upon compressing the two-phase system, which results in increasing the solubility of gas in liquid, and rapid reduction of pressure causing micro- and nanobubble generation (Terasaka et al., 2011). The most common methods belong to gas-liquid circulation group. When using these methods, one pressurizes the gas into pre-generated liquid flow or vortex. The bubbles are formed by cutting them of the surface by shear stress caused by the liquid flow or centrifugal force (Terasaka et al., 2011). One of these methods is generation by means of porous membrane modules, which will be described further below.

Generation of nanobubbles using porous membranes is possible, but requires the knowledge and understanding of phenomena that accompany transfer of gas through pores of micrometric size. Immersing the membrane in liquid and pressurizing gas through pores is not sufficient for generating bubbles in micro- and nanoscale (Zimmerman et al., 2008). During the formation of bubbles on the membrane surface, the surface tension and adhesion forces prevent bubbles from breaking off the membrane surface, which makes them grow in size by filling them with more and more gas. If this adhesion is not impeded by any means, the growing will continue until the buoyancy overcomes the forces of adhesion. That leads to generation of bubbles whose sizes are even two magnitudes larger than the diameter of membrane pores (Zimmerman et al., 2008). Because of this fact, it is essential to generate the turbulence or shear stress which will help overcoming the adhesion and allow cutting the bubbles off the membrane surface (see Fig. 1.). The easiest way to generate higher shear stress is to increase the flowrate of liquid. For that reason, the investigation of liquid flowrate increase on the size of nanobubbles was performed. The literature presents some results which try to capture the essence of this phenomenon. Khirani et al. (2012) performed microbubble generation in water and heptane using alumina based membranes with pore diameter of 800 nm and 100 nm or zirconium oxide based membranes with pore diameter of 20 nm and 100 nm (Khirani et al., 2012).

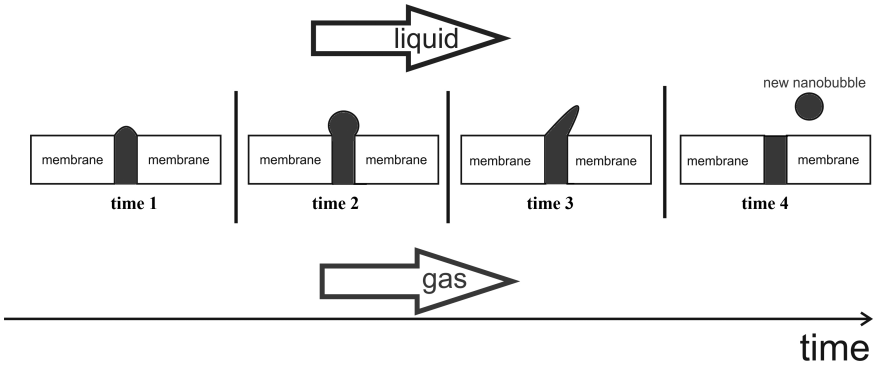

Fig. 1. Scheme of nanobubble generation mechanism by porous membranes

Unfortunately, researchers gathered information mostly for bubbles larger than 1 μm, so we cannot be sure, whether they obtained nanobubbles. Nevertheless, they reported that applying shear stress of even 7 Pa allowed the bubbles to detach from the membrane surface earlier which resulted in lower diameter of such bubbles, than when no shear stress was applied (Khirani et al., 2012). Kukizaki and Goto (2006) performed the generation of bubbles using SPG (Shirasu Porous Glass) membranes with various pore diameters ranging from 43 nm to 85 nm (for investigation of influence of pore diameter on bubble diameter) and from 55 nm to 2.23 μm (for investigation of influence of shear stress on the diameter of generated bubbles). They also have shown that applying even low shear stress (under 15 Pa) resulted in the reduction of bubble size. However, their investigation showed that the size of bubbles remains constant for higher shear stress (up to 50 Pa, which was the highest investigated shear stress) (Kukizaki and Goto, 2006).

Another fact, which is important when one considers overcoming the adhesion of bubbles, is wettability of surface and in consequence the contact angles of bubble on the membrane surface. Hydrophobic membranes (characterized by a low wettability) have an advantage of adhering gas to membrane surface when polar liquids, such as water are used. It is caused because the adhesion forces between membrane surface and liquid are much lower than the cohesion forces of liquid, thus allowing the bubble to cover larger area of the membrane surface and to be more resistant to shear stress (Kukizaki and Wada, 2008; Zimmerman et al., 2008). So it is necessary to use membranes of wettability adequate to polarity of the liquid used.

2. MATERIALS AND METHODS

2.1. Porous-membrane modules

During the experiments, two different porous membrane modules (pore diameter 0.2 μm) were used (denoted as Module 1 and Module 2, respectively). Module 1 was made of 98% porous silicon carbide with 31 round channels (Ø 3 mm). Module 2 contained single porous-membrane tube (internal/external diameter of 6 mm/16 mm) inside stainless steel external tube. Silicon carbide is characterized by high wettability (contact angles −45–50 ° (Zhong et al., 2016)).

2.2. Experimental set-up

Figure 2 shows the scheme of experimental setup. Deionized water stored in tank is pumped by centrifugal pump and flows to inner tube/channels of porous-membrane module. Pressurized nitrogen from a cylinder flows through pores of the membrane to the flowing liquid, which cuts off bubbles forming onto the membrane surface. The water containing nanobubbles is returned to the storage tank.

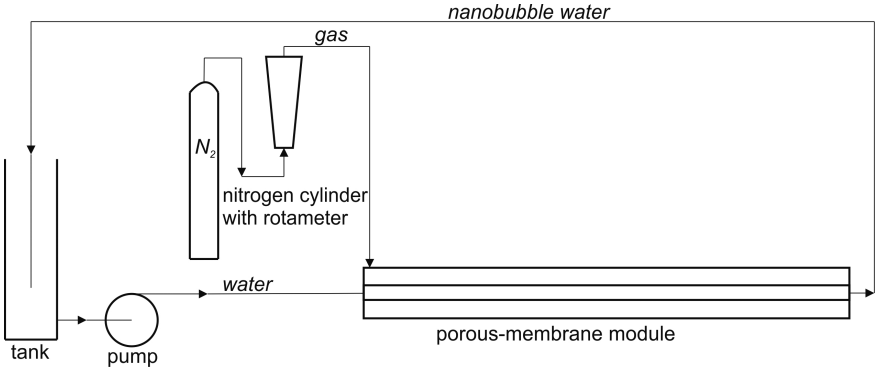

Fig. 2. Scheme of experimental setup

For each module, two distinct liquid flowrates were chosen and each experiment was labelled with subsequent numbers, as shown in Table 1. Each generation charge lasted 2 hours after which two samples were collected. Three charges were performed for each experiment.

Table 1. Flowrates of media for performed experiments

Module	Experiment	Liquid flowrate, [dm^3h^{-1}]	Gas flowrate, [dm^3h^{-1}]
Module 1	Experiment 1	1900	850
Module 1	Experiment 2	950	850
Module 2	Experiment 3	900	200
Module 2	Experiment 4	600	200

2.3. Size distribution measurement

Size distribution of bubbles in samples was measured using Malvern Zetasizer Nano using Dynamic Light Scattering (DLS) technique. This technique enables correlating the rate of change of scattered light spectrum with diffusion rate of dispersed objects. Next, to obtain the size of the mentioned objects in the liquid, the Stokes–Einstein equation is used:

$$D = \frac{k_B \cdot T}{3\pi \cdot \mu \cdot d} \tag{2}$$

For each sample, three measurements were performed and the mean Sauter diameter (d_{32}) was calculated according to Eq. (3).

$$d_{32} = \frac{\sum n_i d_i^3}{\sum n_i d_i^2} \tag{3}$$

Three obtained Sauter diameter values were averaged to acquire the value of the mean diameter in given sample.

3. RESULTS AND DISCUSSION

Size distributions of nanobubbles for each of all four experiments were obtained and displayed in Figs. 3–6. As can be seen, the generated nanobubbles are of polydisperse character. For System 1 (Figs. 3 and 4) there is no definite single dominant fraction, the distribution is very wide and has numerous maxima. For System 2 (Figs. 5 and 6) one can observe a dominant fraction of diameter in the range of 400–600 nm. That may indicate that higher roughness of the membrane surface favors generation of bubbles of a single diameter. It is also important to note, that for Experiments 2 and 4 (Fig. 4 and 6), which were performed using lower water flow rates, bubbles of larger diameter than for Experiments 1 and 3, where water flow rates were higher, can be observed.

In Figs. 7–9, the values of the mean Sauter diameter were presented. Figure 7 shows results obtained for Experiment 1 (water flow rate of 32 dm^3/min) and Experiment 2 (water flow rate of 16 dm^3/min). In Fig. 8, one can see the results for Experiment 3 (water flow rate of 15 dm^3/min) and Experiment 4 (water flow rate of 10 dm^3/min). Each bar represents results acquired for one generation charge for every experiment. The averaged results for each experiment are displayed in Fig. 9.

As one can see in Figs. 7 and 8, at higher value of liquid flow rate, the mean diameter of bubbles and the value of standard deviation are lower. That fact is even more visible in Fig. 9. It should be noted that

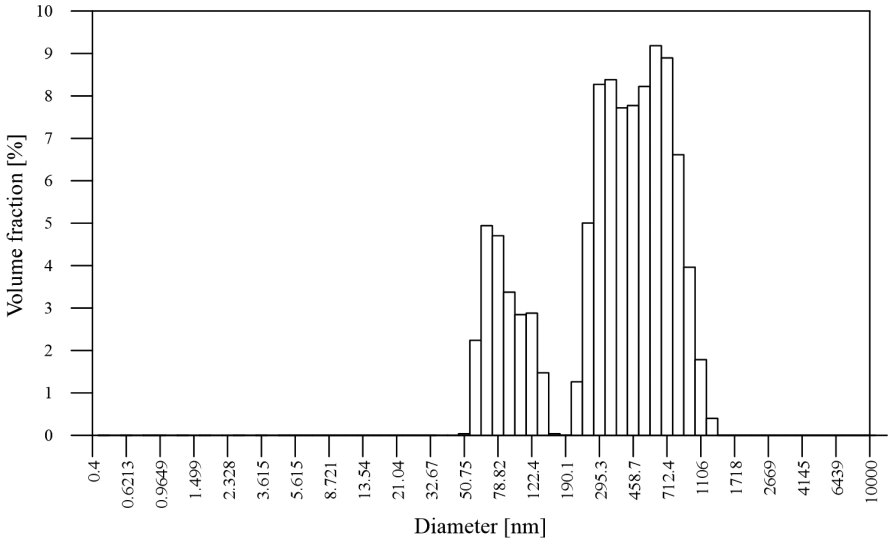

Fig. 3. Size distribution of bubbles obtained in Experiment 1, System 1 (water flow rate of 32 L/min

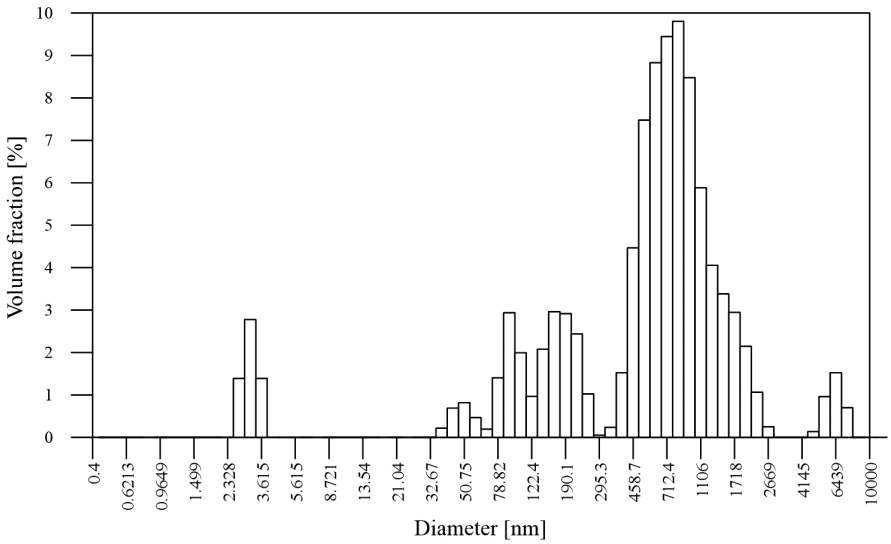

Fig. 4. Size distribution of bubbles obtained in Experiment 2, System 1 (water flow rate of 16 L/min)

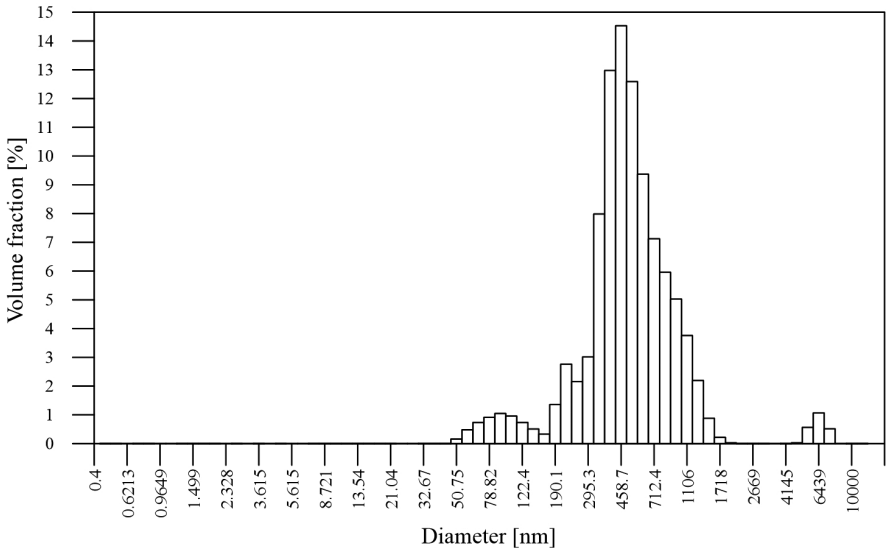

Fig. 5. Size distribution of bubbles obtained in Experiment 3, System 2 (water flow rate of 15 L/min)

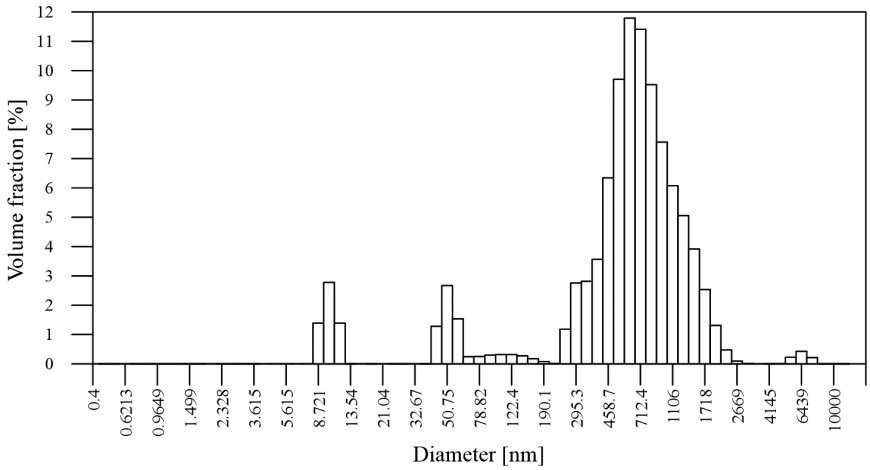

Fig. 6. Size distribution of bubbles obtained in Experiment 4, System 2 (water flow rate of 10 L/min)

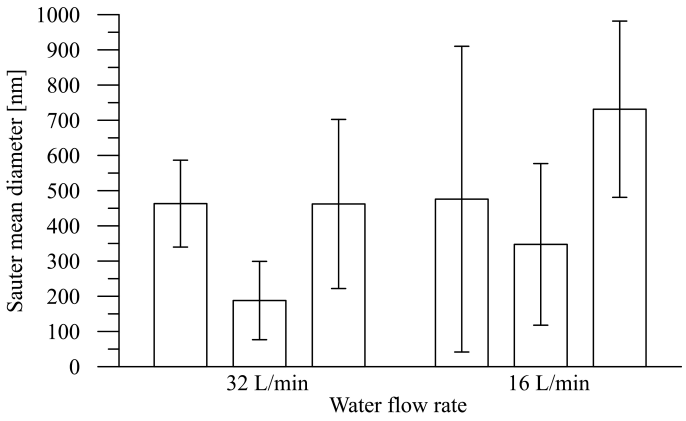

Fig. 7. Sauter mean diameter of bubbles for Experiment 1 (left, 32 L/min) and Experiment 2 (right, 16 L/min). Each bar represents distinct generation charge

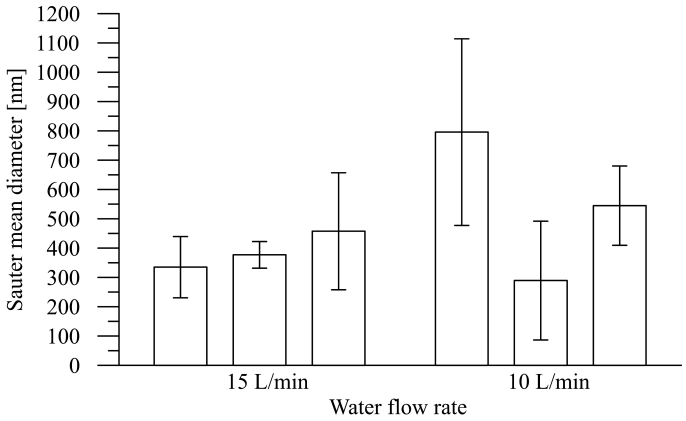

Fig. 8. Sauter mean diameter of bubbles for Experiment 3 (left, 15 L/min) and Experiment 2 (right, 10 L/min). Each bar represents distinct generation charge

despite being placed in the same figure, two leftmost bars represent experiments performed in System 1, and two rightmost ones represent experiments performed in System 2, respectively.

To correctly interpret the results of our experiments, we should analyse the regime of the liquid flow. For that we calculated the Reynolds number for each of the experiments according to Equation (4) (Table 2).

$$Re = \frac{u d_H \rho}{\mu} \tag{4}$$

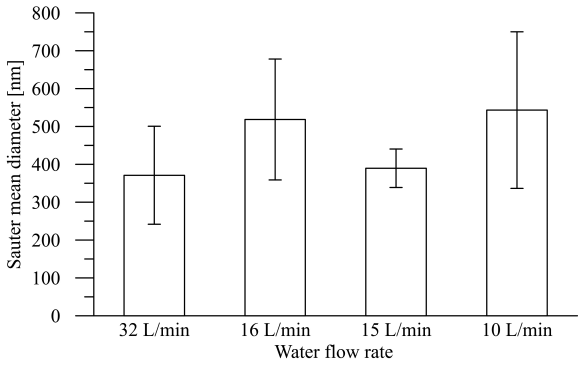

Fig. 9. Averaged results of Sauter mean diameter of bubbles for each experiment. From left to right: Experiment 1, Experiment 2, Experiment 3, Experiment 4

Table 2. Values of volumetric flow rate, superficial velocity and Re number for each experiment

Name	$Q{\cdot}10^4$ [m^3/s]	u [m/s]	Re [–]
Experiment 1	5.28	2.41	72126
Experiment 2	2.64	1.20	36063
Experiment 3	2.50	8.84	529561
Experiment 4	1.67	5.89	353041

Next step is obtaining the information about shear stress τ in a channel. To do so, we use Darcy–Weisbach equation (Eq. (5)).

$$\tau = \frac{1}{8}\lambda\,\rho\,u^2 \tag{5}$$

As all Reynolds numbers are suggested to develop turbulent flow, friction factor λ can be evaluated using Blasius approximation for Re from 10^3 to 10^6:

$$\lambda = 0.3164\,Re^{-0.25} \tag{6}$$

Using Equations (4)–(6), we obtain the values of shear stress for each experiment (Table 3).

Table 3. Values of Re number, friction factor and shear stress for each experiment

Name	Re [–]	λ [–]	τ [Pa]
Experiment 1	72126	0.019	13.9
Experiment 2	36063	0.023	4.15
Experiment 3	529561	0.012	114
Experiment 4	353041	0.013	56.3

As one can see, for the Module 1 (Experiments 1 and 2) the shear stress calculated in that way is much lower than that for the Module 2 (Experiments 3 and 4). However, one cannot be sure whether in Module 1 (31 cylindrical channels 3 mm in diameter) the effect of low radius does not produce higher shear stress because of the surface roughness. Nevertheless, our studies confirm the results obtained by both Kukizaki and Goto (2006) and by Khirani et al. (2012), that applying even low shear stress results in the change of generated bubbles, as we can see in results from Module 1. However, we also showed that applying high

shear stress (56 to 114 Pa) results in further decrease of bubble diameter which was not investigated by the above mentioned researchers. We can assume that higher values of liquid flowrate allow for generating smaller bubbles because they are subject to higher shear stress. For that reason, bubbles can be cut off from the membrane surface earlier, i.e. before they are able to grow. Applying low values of shear stress results in cutting of the bubbles that have diameter over twice the size of the pore, as shown by Kukizaki and Goto (2006). For membrane pores of 100 nm they obtained bubbles of size about 500 nm. After that they observe the constancy of bubble diameter which does not change with increasing shear stress up to 50 Pa. That value is consistent with our research for shear stress of 56 Pa. However, as we have shown in this paper, further increase of shear stress (up to 114 Pa) results in obtaining smaller bubbles. Those bubbles are smaller than double the size of membrane pore, which shows that obviously bubbles are cut off from the membrane surface earlier than for shear stress of 56 Pa. What is interesting, one can note in Fig. 9, that for System 1 (Experiments 1 and 2), despite the higher liquid flow rate, bubbles of approximately similar size were obtained. It may be linked to lower roughness of the membrane surface in System 1.

4. CONCLUSIONS

Experiments were performed in two porous-membrane systems for different water flow rates to check whether at higher liquid flow rates bubbles of smaller diameter would be generated. Size distributions and Sauter mean diameters were determined. For both experimental systems smaller bubbles were generated for a higher value of water flow rate and higher shear stress. Additionally, we concluded that higher surface roughness favours generation of smaller bubbles even at lower flow rates.

SYMBOLS

D	diffusion coefficient, $m^2 s^{-1}$
d	bubble diameter, m
d_{32}	Sauter mean diameter, m
d_H	hydraulic diameter of channels in module, m
d_i	diameter of bubbles in fraction i, m
k_B	Boltzmann constant, $J K^{-1}$
n_i	number of bubbles in fraction i, –
Q	volumetric flow rate, $m^3 s^{-1}$
Re	Reynolds number, –
T	temperature, K
u	superficial velocity of the flow, $m s^{-1}$
ΔP	pressure difference, Pa
λ	friction factor, –
μ	dynamic viscosity, Pa s
τ	shear stress, Pa

REFERENCES

Bunkin N.F., Kochergin A.V., Lobeyev A.V., Ninham B.W., Vinogradova O., 1996. Existence of charged submicrobubble clusters in polar liquids as revealed by correlation between optical cavitation and electrical conductivity. *Colloids Surf., A*, 110, 207–212. DOI: 10.1016/0927-7757(95)03422-6.

Cademartiri L., Ozin G.A., Lehn, J.-M., 2009. *Concepts of nanochemistry*. Weinheim, WILEY-VCH, Weinheim.

Chu L.B., Xing X.H., Yu A.F., Zhou Y.N., Sun X.L., Jurcik B., 2007. Enhanced ozonation of simulated dyestuff wastewater by microbubbles. *Chemosphere*, 68, 1854–1860. DOI: 10.1016/j.chemosphere.2007.03.014.

Ebina K., Shi K., Hirao M., Hashimoto J., Kawato Y., Kaneshiro S., Morimoto T., Kozumi K., Yoshikawa H., 2013. Oxygen and air nanobubble water solution promote the growth of plants, fishes, and mice. *PLOS ONE*, 8, 2–8. DOI: 10.1371/journal.pone.0065339.

Etchepare R., Azevedo A., Calgaroto S., Rubio J., 2017. Removal of ferric hydroxide by flotation with micro and nanobubbles. *Sep. Purif. Technol.*, 184, 347–353. DOI: 10.1016/j.seppur.2017.05.014.

Ghosh P., 2009. Coalescence of bubbles in liquid. *Bubble Sci. Eng. Technol.*, 1(1–2), 75–87.

Von Gunten U., 2003. Ozonation of drinking water: Part I. Oxidation kinetics and product formation. *Water Res.*, 37, 1443–1467. DOI: 10.1016/S0043-1354(02)00457-8.

Ikeura H., Kobayashi F., Tamaki M., 2011. Removal of residual pesticide, fenitrothion, in vegetables by using ozone microbubbles generated by different methods. *J. Food Eng.*, 103, 345–349. DOI: 10.1016/j.jfoodeng.2010.11.002.

Khadre M.A., Yousef A.E., Kim J.-G., 2001. Microbiological aspects of ozone applications in food: A review. *J. Food Sci.*, 66, 1242–1252. DOI: 10.1111/j.1365-2621.2001.tb15196.x.

Khirani S., Kunwapanitchakul P., Augier F., Guigui C., Guiraud, P., Hébrard G., 2012. Microbubble generation through porous membrane under aqueous or organic liquid shear flow. *Ind. Eng. Chem. Res.*, 51, 1997–2009. DOI: 10.1021/ie200604g.

Kikuchi K., Tanaka Y., Saihara Y., Maeda M., Kawamura M., Ogumi Z., 2006. Concentration of hydrogen nanobubbles in electrolyzed water. *J. Colloid Interface Sci.*, 298, 914–919. DOI: 10.1016/j.jcis.2006.01.010.

Kobayashi F., Ikeura H., Ohsato S., Goto T., Tamaki M., 2011. Disinfection using ozone microbubbles to inactivate *Fusarium oxysporum* f. sp. *melonis* and *Pectobacterium carotovorum* subsp. *carotovorum*. *Crop Prot.*, 30, 1514–1518. DOI: 10.1016/j.cropro.2011.07.018.

Kukizaki M., Goto M., 2006. Size control of nanobubbles generated from Shirasu-porous-glass (SPG) membranes. *J. Membr. Sci.*, 281, 386–396. DOI: 10.1016/j.memsci.2006.04.007.

Kukizaki M., Wada T., 2008. Effect of the membrane wettability on the size and size distribution of microbubbles formed from Shirasu-porous-glass (SPG) membranes. *Colloids Surf., A*, 317, 146–154. DOI: 10.1016/j.colsurfa.2007.10.005.

Kutty S.R.M., Winarto F.E.W., Gilani S.I.U., Anizam A.A., Karimah W.W.Z., Isa M.H., 2010. Degradation of organic matter using a submerged microbubble diffuser in a biological wastewater treatment system. In: Popov V., Itoh H., Mander U., Brebbia C.A. (Eds.). *Waste Management and the Environment V*. WIT Press, USA, 1, 415-423.

Li H., Hu L., Song D., Lin F., 2014. Characteristics of micro-nano bubbles and potential application in groundwater bioremediation. *Water Environ. Res.*, 86, 844–851. DOI: 10.2175/106143014X14062131177953.

Matsumoto M., Tanaka K., 2008. Nano bubble-size dependence of surface tension and inside pressure. *Fluid Dyn. Res.*, 40, 546–553. DOI: 10.1016/j.fluiddyn.2007.12.006.

Park J.S., Kurata K., 2009. Application of microbubbles to hydroponics solution promotes lettuce growth. *HortTechnol.*, 19(1), 212–215.

Sreekanth R., Prasanthkumar K.P., Sunil Paul M.M., Aravind U.K., Aravindakumar C.T., 2013. Oxidation reactions of 1- and 2-naphthols: An experimental and theoretical study. *J. Phys. Chem. A*, 117, 11261–11270. DOI: 10.1021/jp4081355.

Srinivas A., Ghosh P., 2012. Coalescence of bubbles in aqueous alcohol solutions. *Ind. Eng. Chem. Res.*, 51, 795–806. DOI: 10.1021/ie202148e.

Sunil Paul M.M., Aravind U.K., Pramod G., Aravindakumar C.T., 2013. Oxidative degradation of fensulfothion by hydroxyl radical in aqueous medium. *Chemosphere*, 91, 295–301. DOI: 10.1016/j.chemosphere.2012.11.033.

Takahashi M., 2009. Base and technological application of micro-bubble and nanobubble. *Mater. Integration*, 22, 2–19.

Terasaka K., Hirabayashi A., Nishino T., Fujioka S., Kobayashi D., 2011. Development of microbubble aerator for waste water treatment using aerobic activated sludge. *Chem. Eng. Sci.*, 66, 3172–3179. DOI: 10.1016/j.ces.2011.02.043.

Tsuge H., 2015. *Micro- and nanobubbles. fundamentals and applications*. Pan Stanford Publishing.

Xiao Q., Liu Y., Guo Z., Liu Z., Zhang X., 2017. How nanobubbles lose stability: Effects of surfactants. *Appl. Phys. Lett.*, 111, 131601. DOI: 10.1063/1.5000831.

Zhang L.J., Chen H., Li Z.X., Fang H.P., Hu J., 2008. Long lifetime of nanobubbles due to high inner density. *Sci. China, Ser. G*, 51, 219–224. DOI: 10.1007/s11433-008-0026-5.

Zhong W.W., Huang Y.F., Gan D., Xu J.Y., Li H., Wang G., Meng S., Chen L., 2016. Wetting behavior of water on silicon carbide polar surfaces. *Phys. Chem. Chem. Phys.*, 18, 28033–28039. DOI: 10.1039/C6CP04686J.

Zimmerman W.B., Tesař V., Butler S., Bandulasena H.C.H., 2008. Microbubble Generation. *Recent Pat. Eng.*, 2, 1–8. DOI: 10.2174/187221208783478598.

Received 24 May 2018
Received in revised form 25 July 2018
Accepted 04 September 2018